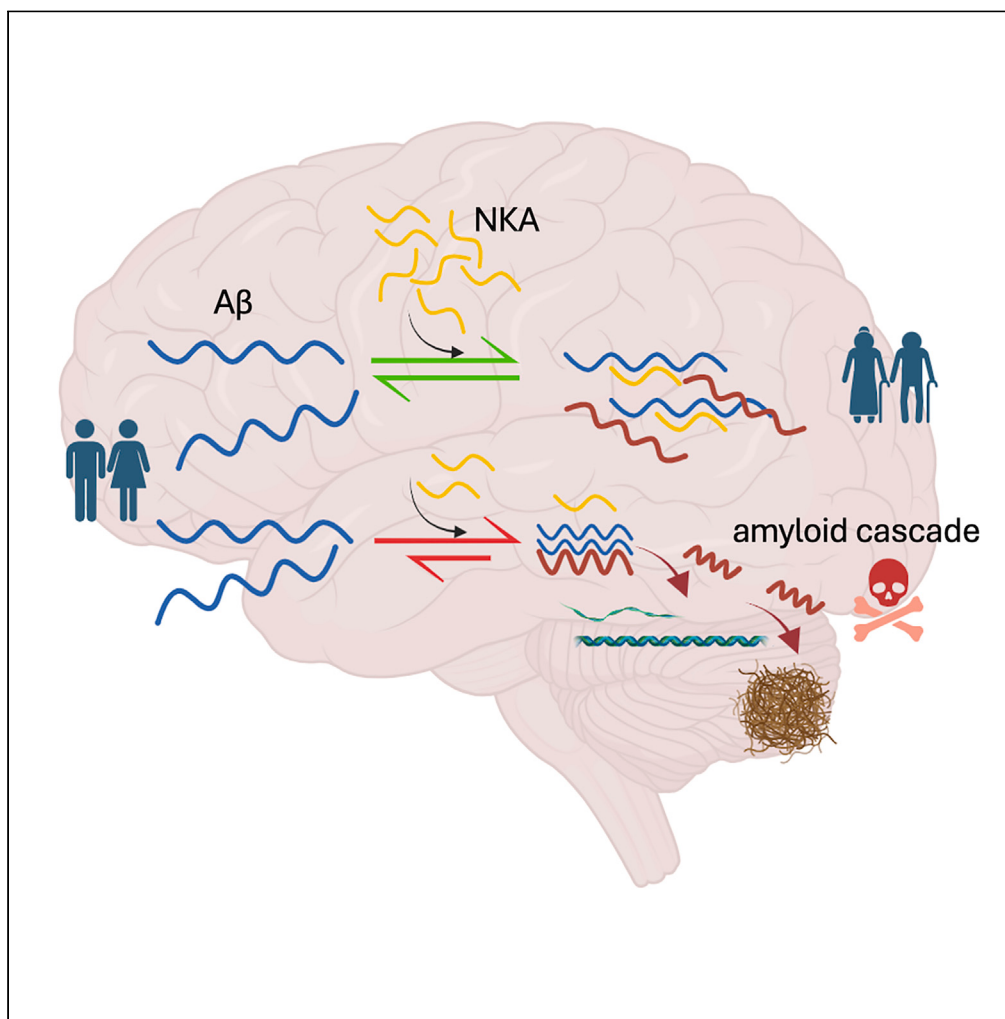


Article

Decoding the molecular and structural determinants of the neuropeptide NKA and $\text{A}\beta_{1-42}$ peptide cross-interaction in the amyloid cascade pathway

Mohsen Habibnia,
Eric Catalina-
Hernandez, Mario
Lopez-Martin,
David Masnou-
Sanchez, Alex
Peralvarez-Marin

alex.peralvarez@uab.cat

Highlights

NKA and $\text{A}\beta_{1-42}$ computational model shows that peptide-peptide cross-interact

The NKA and $\text{A}\beta_{1-42}$ cross-interaction is mediated by aromatic and hydrophobic residues

In vitro, NKA influences the $\text{A}\beta_{1-42}$ aggregation in a concentration-dependent manner

NKA presence ameliorates the toxicity of $\text{A}\beta_{1-42}$ in SH-SY5Y cultured cells

Habibnia et al., iScience 27,
111187
November 15, 2024 © 2024 The
Authors. Published by Elsevier
Inc.
<https://doi.org/10.1016/j.isci.2024.111187>



Article

Decoding the molecular and structural determinants of the neurokinin A and A β ₁₋₄₂ peptide cross-interaction in the amyloid cascade pathway

Mohsen Habibnia,^{1,2,3} Eric Catalina-Hernandez,^{1,2,3} Mario Lopez-Martin,^{1,2,3} David Masnou-Sanchez,^{1,2} and Alex Peralvarez-Marín^{1,2,4,*}

SUMMARY

Tachykinins are short neuropeptides, such as substance P and neurokinin B, that have been shown to interact with Alzheimer's β -amyloid (A β) peptide. Neurokinin A (NKA) is a secreted tachykinin neuropeptide that binds to neurokinin receptors and with an emerging role in the brain-gut axis. NKA shares the brain niche with A β ; thus, we investigate whether and how NKA and A β peptide interact. We have used a combination of computational and experimental biophysics to assess the interaction of both peptides *in vitro*. Using Phe-to-Trp substitution, we have shown that Phe in the FXGLM signature in NKA is important for such interaction and for the modulation of the A β peptide amyloid cascade. Besides, cellular experiments have shown that the NKA-A β interaction decreases the A β peptide toxicity. Altogether, our work raises the intriguing possibility that NKA balance and the NKA-A β peptide interplay are relevant in the aggregation process in Alzheimer's disease.

INTRODUCTION

Alzheimer's disease (AD) as a neurodegenerative disorder is the major cause of elderly dementia and the most prevalent form of amyloidosis with aging as its most significant risk factor.¹ Monomeric soluble β -amyloid (A β) peptides aggregate into β sheet-rich oligomers and insoluble fibrils into extracellular senile A β plaques²⁻⁴ resulting in oxidative stress, neuronal loss, blood-brain barrier breakdown, synaptic dysfunction, and metal homeostasis disturbance leading to neuronal death.⁵⁻⁸

Neuropeptides as molecules coexisting with A β peptides are key potential interactors for A β and, more importantly, putative enhancers, chelators, and/or buffers of the amyloid potential of this peptide, as it has been shown in several peptide homo and hetero-cross-interactions,⁹⁻¹² such as dynorphins¹³ or tachykinins (TKs),¹⁴ both of them related to the brain-gut axis.^{15,16} The progression of A β fibril development occurs during the aggregation process, with monomers of A β serving as seeds for nucleation in the initial phase. Overcoming the challenge of preventing or inhibiting the formation of toxic early-stage dimers is complex, given the myriads of physiological factors that can either promote or inhibit this process, depending on the physiological state. In fact, the study of peptide cross-interactions not only allows a better understanding of the pathophysiology of neurodegenerative disorders^{12,17} but also opens a rational-design window to define peptide-based therapy and diagnosis strategies.¹⁸

Mammalian TKs are a family of neuropeptides broadly expressed in neuronal and nonneuronal tissues.¹⁹ TK target receptors are vastly localized in the brain, and these neuropeptides function as neurotransmitters in different biological activities including pain processing, neuroinflammation, hormone regulation, immune function, and memory formation,^{20,21} and more recently on the spot of the brain-gut axis.²² The three foremost TK members in mammalian species are substance P (SP), neurokinin A (NKA), and neurokinin B (NKB), which consist of 10–12 residues sharing the conserved motif FXGLM in the C-terminal region (X, hydrophobic residue, Table 1).²³ The cerebrospinal fluid tachykinergic system's functionality is altered in patients suffering from AD, as it has been indicated that TK levels, as well as their immunoreactivity, are decreased in the brains of patients with AD.^{24,25} It has been shown that SP and NKB are able to interact with A β and modulate the amyloid cascade.^{14,26,27} A β and TK peptides coexist in the brain parenchyma and cross-interact affecting AD progression. Several studies have indicated the neuroprotective effects of TKs in AD both *in vivo* and *in vitro*.²⁸⁻³² NKA is ubiquitously expressed in the central and peripheral nervous system, released from the nerve endings and acting as a neurotransmitter and neuromodulator in various neurophysiological activities,³³ with high affinity to type 2 neurokinin receptor.³⁴ NKA has been recently related to the brain-gut axis connection in neurodegenerative disorders.^{35,36}

¹Unit of Biophysics, Department of Biochemistry and Molecular Biology, Facultat de Medicina, Universitat Autònoma de Barcelona, 08193 Cerdanyola del Vallès, Catalonia, Spain

²Institute of Neurosciences, Universitat Autònoma de Barcelona, 08193 Cerdanyola del Vallès, Catalonia, Spain

³These authors contributed equally

⁴Lead contact

*Correspondence: alex.peralvarez@ub.cat
<https://doi.org/10.1016/j.isci.2024.111187>



Table 1. Peptide physico-chemical properties

Peptide	Primary sequence	Mol. weight ^a	pI ^a	Charge ^a	GRAYV Index ^a
A β_{1-42}	DAEFRHDSGYEVHHQKLF FAEDVGSNKGAIIGLMVGGVIA	4,514.1	5.3	-3	0.20
NKA	HKTDSFVGLM-NH ₂	1,134.3	6.7	0	0.02
NKAW	HKTDSWVGLM-NH ₂	1,173.3	6.7	0	-0.35
NKB	DMHDFFVGLM-NH ₂	1,211.4	4.2	-2	0.68
Substance P	RPKPQQFFGLM-NH ₂	1,348.63	11.0	+2	-0.70

^aAnalysis performed using Expasy ProtParam tool.³⁷

Comprehensive assessment of the molecular and structural determinants of cross-interactions is imperative, considering their potential positive, negative, or neutral impact on the amyloid pathway. In the present study, we complement computational simulations to characterize the NKA-A β_{1-42} cross-interaction with *in vitro* biophysical characterization and cell toxicity experiments to determine the influence of NKA over the A β amyloid pathway, which may open rational-design window to define peptide-based therapy and diagnosis strategies for NKA.

RESULTS

Building the NKA-A β dimer

In this study, we investigate the cross-interaction between NKA and A β . To establish an unbiased system, we employ peptide-peptide docking (Figure 1A), aiming to acquire an unsupervised configuration for the NKA-A β heterodimer as the starting point for our simulation (Figure 1B at 0 ns). The main contacts are between Glu22, Leu34, Met35, and Val39 in A β_{1-42} , and His1 and Lys2 in NKA, respectively (Figure 1B). We use the available structural information for A β_{1-42} , such as the random coil structure (PDB: 6SZF, Figure 1B) and the helical structure (PDB: 1IYT, Figure S1) to define the reference for secondary structure-dependent amyloid aggregation in solution. First, we use two randomly positioned A β monomers to observe the amyloid interaction between both monomers within a 1 μ s simulation (Figures 1B and S1). In parallel, we follow the behavior of two stoichiometries for NKA: A β (Figure 1B) using all-atom molecular dynamics for 1 μ s.

NKA stabilizes helical structure in A β_{1-42}

In the absence of NKA, random coil A β_{1-42} collapses into a dimer and defines a cluster of mostly random coil structure, a region of helical structure, and scattered β -structure hotspots throughout the peptide (Figure 2A). In the presence of NKA, A β_{1-42} helical secondary structure is favored in the central core (residues 23–30) of one A β_{1-42} monomer at 2:1 (Figure 2B) and in both A β_{1-42} monomers at 2:2 (Figure 2C) stoichiometries, respectively. Figure S2 shows the structural propensities in simulations carried out with helical A β_{1-42} peptide as starting model. Within the 1 μ s time frame, the A β_{1-42} dimer loses helical structures in favor of random coil and turn structures, together with the onset of β

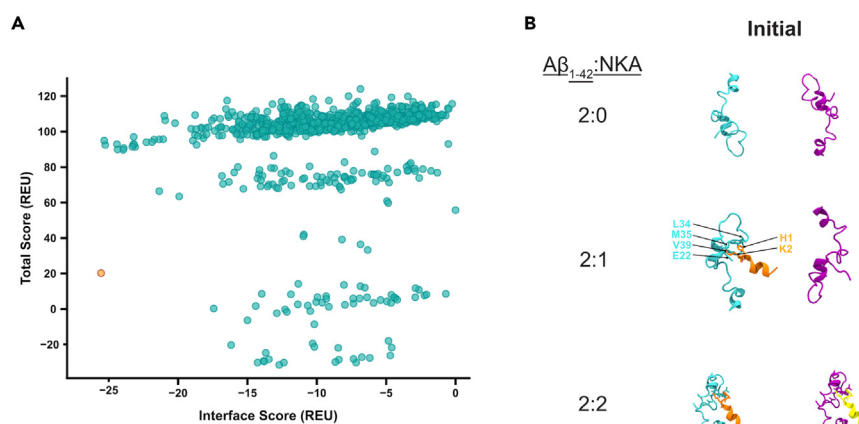


Figure 1. Peptide-peptide docking and time-specific snapshots of the simulation

(A) Most stabilized docking pose is chosen (indicated in orange) by cross-correlation coefficient. REU, Rosetta energy units.

(B) Initial MD simulation snapshots of A β_{1-42} dimer and A β_{1-42} -NKA peptide complex at indicated stoichiometries. A β_{1-42} peptides are depicted in cyan and NKA peptides are depicted in orange and yellow.

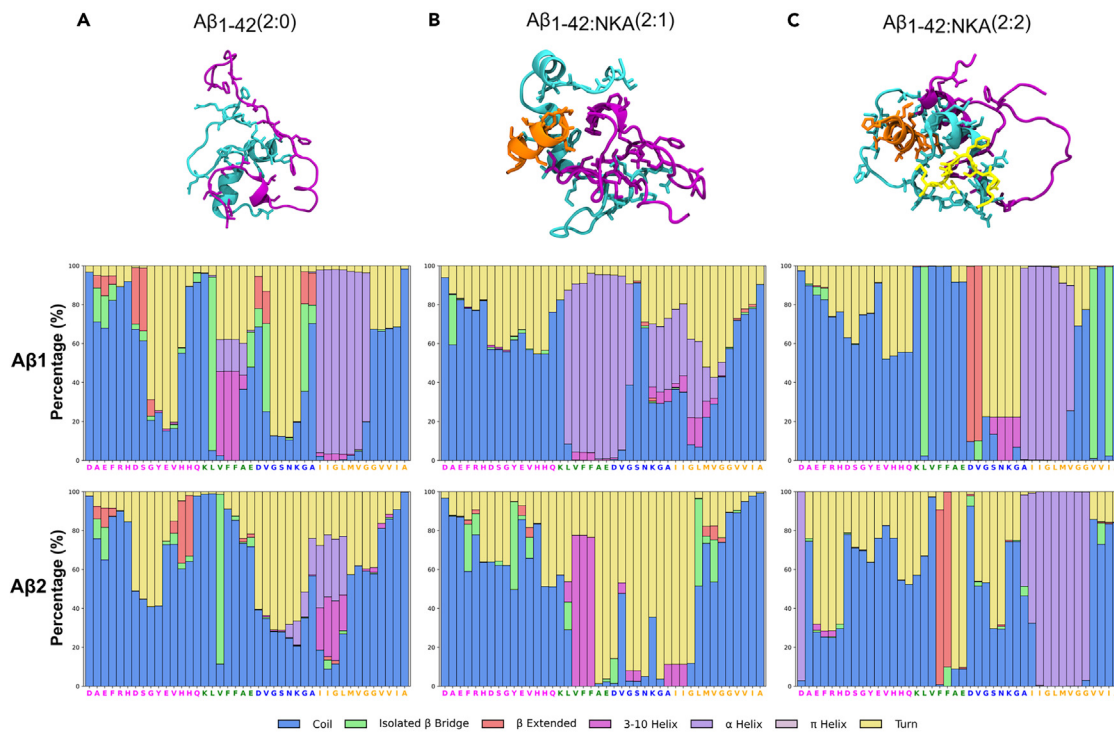


Figure 2. Secondary structure propensities of A β ₁₋₄₂ induced by NKA cross-interaction

A β 1 and A β 2 together as A β ₁₋₄₂ dimer and their secondary structure conversion with a total simulation contact time of the last 500 ns of the simulation for: (A) A β ₁₋₄₂ dimer (2:0), (B) A β ₁₋₄₂-NKA (2:1), and (C) A β ₁₋₄₂-NKA (2:2). On top, molecular illustration of the most representative cluster of the last 500 ns of the simulation. A β ₁₋₄₂ peptides are depicted in cyan and purple and NKA peptides are depicted in orange and yellow. A β ₁₋₄₂ domains are indicated following the color code: N-terminal unstructured domain (residues 1 to 15) in magenta; primary hydrophobic core (residues 16 to 22) in green; central core (residues 23 to 30) in blue; and C-terminal hydrophobic core (residues 31–42) in yellow.

sheet-related spots (bridge and extended) in the C terminus. The presence of NKA at both stoichiometries stabilizes the helical A β ₁₋₄₂ structure at the central, secondary, and C-terminal hydrophobic cores in A β ₁₋₄₂ (Figure S2).

Regardless of using a random coil (Figure 3A) or helical (Figure S3) for A β ₁₋₄₂ structure, there are several hydrophobic-driven contacts between monomers that result into the amyloid dimer. Once NKA comes into play, the tachykinin neuropeptide prevents certain A β ₁₋₄₂ dimer contacts at both stoichiometries (2:1 and 2:2, Figures 3B and 3C, respectively; Figure S3). Specific NKA interactions occur between the NKA FVGLM signature and the first hydrophobic core (K₁₆L₁₇V₁₈F₁₉E₂₀) in A β ₁₋₄₂, through π - π interactions driven via the single aromatic NKA Phe residue (Figures 3D and 3E), but also preventing the inter and/or intra A β ₁₋₄₂ salt bridge formation between Asp23 and Lys28, important for the A β ₁₋₄₂ self-assembly.³⁸ The role of Phe has been previously emphasized as a key residue in amyloid interactions,^{39,40} as also shown for NKB,¹⁴ with two Phe residues in the FVGLM signature.

Phe residue is key in the NKA-A β ₁₋₄₂ interaction

Accordingly, we took advantage of the computational approach to dissect the role of the single Phe residue in NKA, by the Phe-Trp conservative substitution, subsequently named NKAW (Figures 4A and S1). Regarding A β ₁₋₄₂ dimer secondary structure propensities, NKAW stabilizes the helical structures throughout A β ₁₋₄₂ at the 2:1 and at the 2:2 stoichiometries (Figure 4B) when we use random coil A β ₁₋₄₂ as starting point. In simulations using the helical A β ₁₋₄₂, higher β -structure propensities are observed in the A β monomers (Figure S2). The Phe-Trp substitution allows the interaction of NKAW Trp with the K₁₆L₁₇V₁₈F₁₉E₂₀ hydrophobic core of A β ₁₋₄₂ at 2:1 stoichiometry, but to a lesser extent in the 2:2 stoichiometry (Figures S4 and S5 for A β ₁₋₄₂ random coil and helical initial structures, respectively).

As a summary, in Figure 5, we show the aromatic interactions driven by Phe/Trp in NKA and NKAW with Phe19 and Phe20 in A β ₁₋₄₂, using random coil (Figure 5A) or helical (Figure 5B) structures. Regardless the initial conformation of A β ₁₋₄₂, in the absence of NKA/NKAW, Phe19 and Phe20 of A β ₁₋₄₂ monomers are able to interact through π - π stacking. When NKA/NKAW comes into play, Phe6/Trp6 reorients away one of the Phe in the 19–20 di-Phe motif, preventing a tight π - π stacking interaction between A β ₁₋₄₂ monomers.

Effect of NKA/NKAW interaction on the A β ₁₋₄₂ amyloid pathway

First, to determine that the Phe-Trp substitution did not affect the structure of the peptide, we analyzed the circular dichroism (CD) behavior of both NKA and NKAW using thermal ramps, resulting in no significant structural differences (Figure S5). To obtain further details

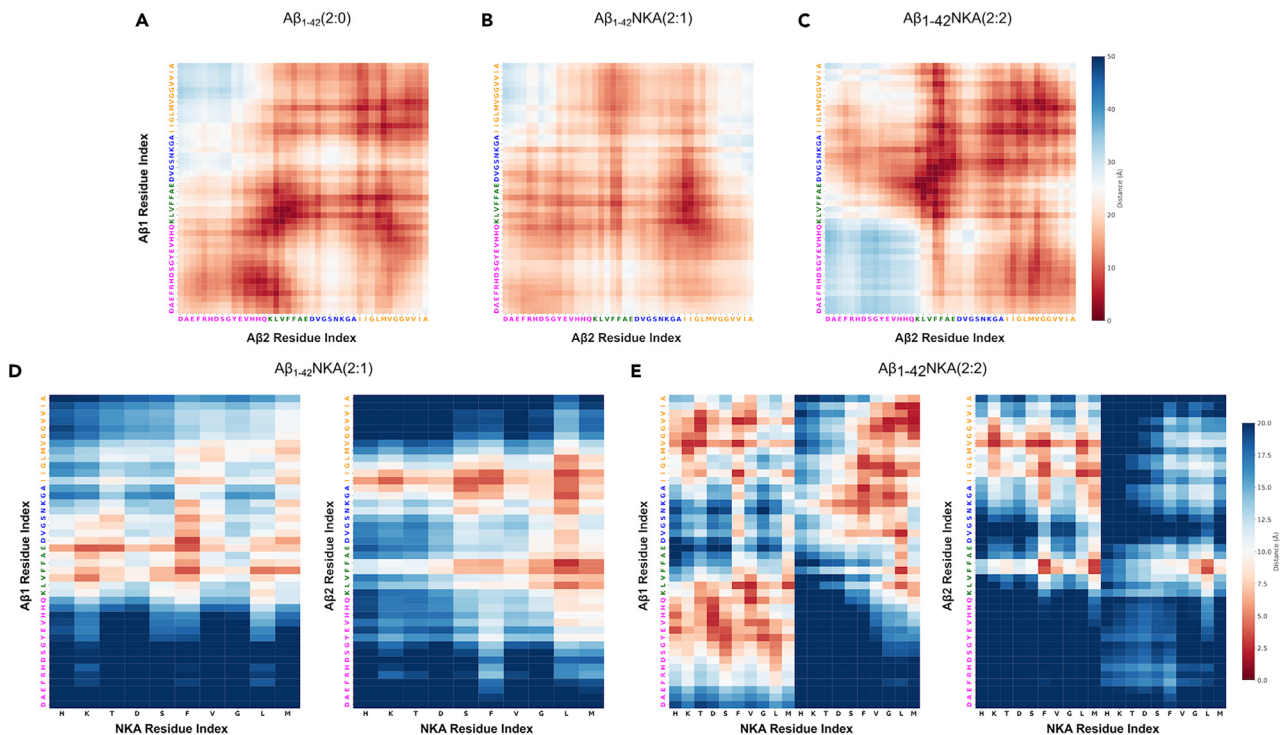


Figure 3. Residue-residue contacts map of the 1 μ s simulation

Intermolecular residue-residue contacts for A β ₁₋₄₂ dimer interaction in the absence (A), at (A β ₁₋₄₂:NKA, 2:1) (B), and at (A β ₁₋₄₂:NKA, 2:2) (C) stoichiometries. (D) NKA-A β contacts map for 1 NKA peptide in the presence of two A β ₁₋₄₂ peptides (A β ₁₋₄₂:NKA, 2:1). (E) NKA-A β contacts map for two NKA peptides in the presence of two A β ₁₋₄₂ peptides (A β ₁₋₄₂:NKA, 2:2). A β ₁₋₄₂ domains are indicated following the color code: N-terminal unstructured domain (residues 1 to 15) in magenta; primary hydrophobic core (residues 16 to 22) in green; central core (residues 23 to 30) in blue; and C-terminal hydrophobic core (residues 31–42) in yellow.

of the NKA/NKAW-A β ₁₋₄₂ interactions, thioflavin T (ThT) fluorescence labeling was used to monitor aggregation kinetics for A β ₁₋₄₂ alone and in the presence of NKA and NKAW at A β ₁₋₄₂:NKA/NKAW stoichiometries 2:1 and 2:2 (Figures 5A and 5B for NKA and NKAW, respectively). Regarding kinetics, the A β ₁₋₄₂ samples incubated with NKA show the highest decrease and slowing down in the amyloid formation process (Figure 6A), as shown by the $\tau_{1/2}$ parameter 12.5 ± 0.4 h ($r_{\max} 1.2 \pm 0.4$ h $^{-1}$) for the samples incubated with NKA at 2:1 stoichiometry, as compared to $\tau_{1/2} 10.5 \pm 0.4$ h ($r_{\max} 0.2 \pm 0.0$ h $^{-1}$) for A β ₁₋₄₂ alone under the same conditions. At 2:2 stoichiometry, NKA decreases the amount of amyloid aggregation but speeds up the kinetics to $\tau_{1/2} 3.7 \pm 0.3$ h (Figure 6A). NKAW (Figure 6B) at 2:1 stoichiometry decreased A β ₁₋₄₂ amyloid formation but sped up the aggregation kinetics to $\tau_{1/2} 6.4 \pm 0.7$ h ($r_{\max} 0.3 \pm 0.1$ h $^{-1}$), with a similar effect at 2:2 stoichiometry with kinetics of $\tau_{1/2} 5.2 \pm 0.4$ h ($r_{\max} 1.2 \pm 0.4$ h $^{-1}$). The samples resulting from the ThT kinetics were observed by transmission electron microscopy, and all the samples containing A β ₁₋₄₂ show a large amount of fibrillar aggregates. Qualitatively, samples containing NKA and NKAW showed smaller fibrillar aggregates. (Figure S6).

β sheet secondary structure of A β ₁₋₄₂ was observed by CD in samples incubated for 1 h, showing a maximum at 203 nm and a minimum at 215 nm (Figure S7). In the presence of NKA and NKAW, the maximum/minimum for β sheet structure was reduced in all cases (Figure S7), indicating an effect due to the presence of both peptides on the secondary structure of A β ₁₋₄₂.

Effect of the NKA-A β ₁₋₄₂ interaction on cell toxicity

Peptide mixtures incubated for at least 24 h were exposed to neuroblastoma-derived cells to assess the toxicity of the aggregates using the 3-(4,5-dimethylthiazol-2-yl)-2,5-diphenyltetrazolium bromide (MTT) assay (Figure 7). Regardless of the peptide-cell interaction mechanism, 10 μ M of A β ₁₋₄₂ exhibits a significant toxicity of 25%, whereas neither NKA nor NKAW showed significant toxicity at 5 or 10 μ M. When cells were treated with the NKA- or NKAW-A β ₁₋₄₂ mixture, cell viability was significantly increased back to normal levels, independently of the stoichiometry used.

DISCUSSION

Amyloid production takes place throughout an individual's lifespan primarily originating from neurons, and with aging as primary risk factor for AD. Peptide cross-interactions, such as A β -TKs,^{26,27,41,42} A β -dynorphins,¹³ and others,^{11,12,18,43,44} act as physiological buffers or enhancers

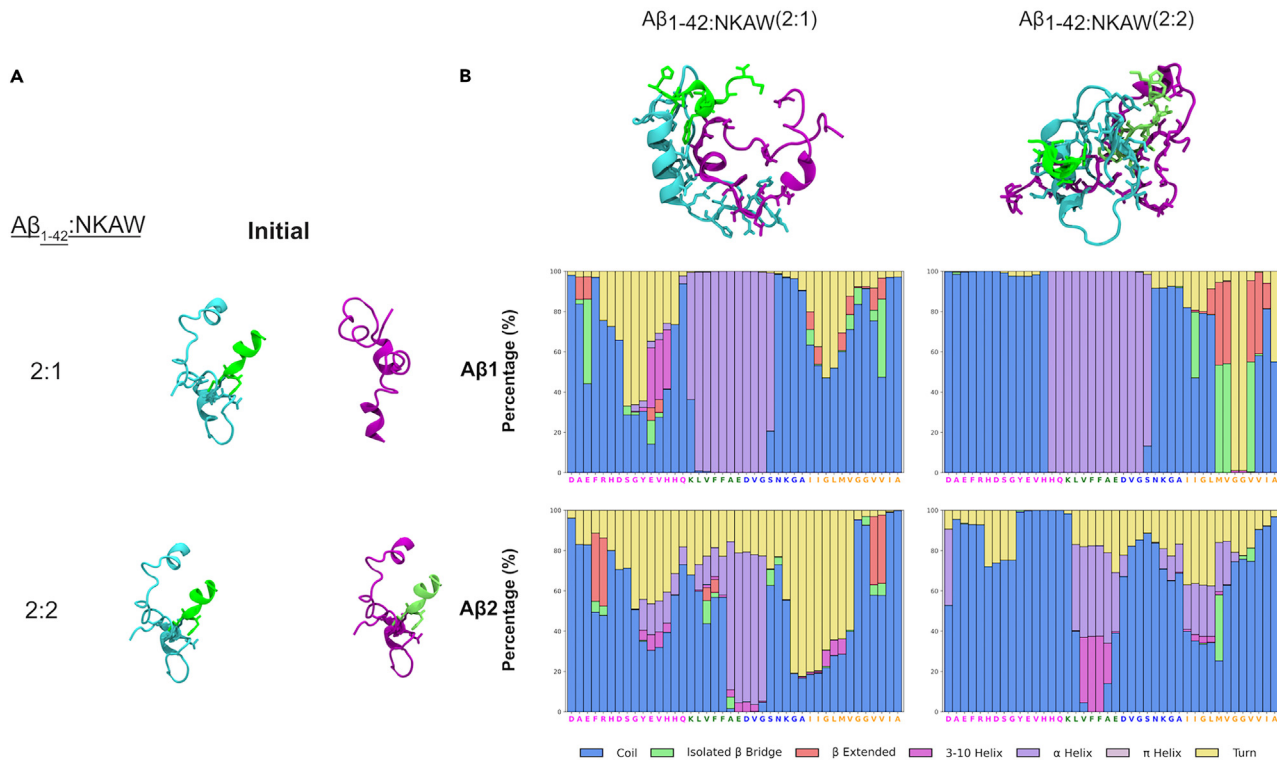


Figure 4. Secondary structure propensities of A β ₁₋₄₂ induced by NKAW cross-interaction

(A) Initial pose of MD simulations of A β ₁₋₄₂ dimer and A β ₁₋₄₂-NKAW peptide complex at indicated stoichiometries. A β ₁₋₄₂ are displayed in cyan and purple and NKAW peptides are depicted in green and light green, respectively.

(B) A β 1 and A β 2 as A β ₁₋₄₂ dimer and their secondary structure conversion with a total simulation contact time of 1 μ s simulation for: A β ₁₋₄₂-NKAW (2:1) and A β ₁₋₄₂-NKAW (2:2). On top, snapshot of the average cluster of the last 500 ns of the MD simulation. A β ₁₋₄₂ domains are indicated following the color code: N-terminal unstructured domain (residues 1 to 15) in magenta; primary hydrophobic core (residues 16 to 22) in green; central core (residues 23 to 30) in blue; and C-terminal hydrophobic core (residues 31–42) in yellow.

for amyloid aggregation. The existence of an age-related pathophysiological condition, characterized by predominant amyloid aggregation within the brain, suggests a potential disruption in peptide cross-interaction homeostasis. This disturbance may lead to the surpassing of the amyloid threshold, consequently exacerbating the onset of the disease beyond reversible limits. Thus, it is key to identify endogenous peptides as A β counterplayers to design strategies for the prevention and inhibition of AD development at all levels. Recent findings demonstrate that dynorphin neuropeptides play a crucial role in inhibiting dimer formation, thereby preventing the initiation of the amyloid cascade and serving as neuroprotectors,¹³ and other neuropeptides, such as NKB, have been found to avoid the A β dimer formation.³⁸ It is reasonable to consider that there exists a physiological inhibition of amyloid aggregation in systemic tissues and the brain, until the concentration of amyloid exceeds a specific threshold leading to the onset of pathology. NKA is especially relevant to understand the brain-gut axis mechanism,²² specifically in the brain. NKA-A β cross-interaction, which has not been so extensively studied compared to other Tks, is likely to occur at physiological level.^{11–13,18,27,43,44} Previous studies show the effect of NKA on the toxic effect of A β at the cellular level,⁴² despite later biochemical and biophysical characterization failed to show any interaction between a Trp-analog for NKA (extra Trp added at the C terminus) and A β ₁₋₄₀.²⁷

Here, to study the NKA-A β cross-interaction, we have used peptides acetylated at the C terminus (both computationally and experimentally), and we use a Trp variant to assess the role of Phe in NKA prior assessment that the secondary structure of the peptide is not affected by the conservative substitution. Then, we complement two approaches, first the computational approach through MD simulations to assess putative molecular determinants in the A β dimer formation, and how the NKA peptide influences this interaction. Previous studies point to the role of the Phe-Phe motif in NKB in stabilizing the NKB-A β cross-interaction through π - π stacking interactions.^{14,17} For NKA, which has a single Phe residue, we observe a similar effect, indicating that interpeptide Phe-Phe π - π stacking is important for the A β self-assembly, but also for A β cross-interactions. To assess the role of the single Phe in NKA in the NKA-A β cross-interaction, we substitute the Phe for a Trp, trying to minimally disturb the cross-interaction, and we observe the NKAW follows the same trend. Our computational results argue that peptides containing aromatic residues act as stabilizers against amyloid self-assembly.⁴⁰

Second, we use biophysics and cell biology to assess the macroscale effects of the NKA-A β cross-interaction. Secondary structure studies using CD indicate a relationship between both peptides (Figure S7), and ThT kinetics show that NKA presence influences the A β aggregation

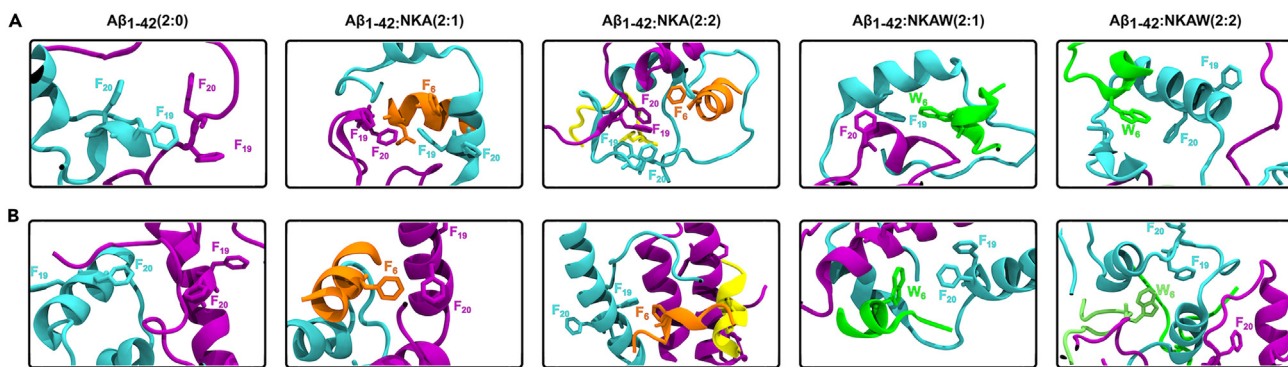


Figure 5. Specific residues mediating the $\text{A}\beta_{1-42}$ -NKA/W A cross-interactions

(A and B) Interaction aromatic residues between $\text{A}\beta_{1-42}$ and NKA/NKAW. The $\text{A}\beta_{1-42}$:NKA/NKAW ratios are: 2:0, 2:1, and 2:2, as indicated. The interactions correspond to the simulations using the NKA/NKAW starting with $\text{A}\beta_{1-42}$ (A) random coil and (B) helical configurations, respectively.

kinetics. The NKA influence is also shown at the cellular level in MTT cell viability assays. The conservative Phe-to-Trp mutation does not affect significantly the *in vitro* and *in cellum* results. Altogether, our results add up to other studies regarding $\text{A}\beta$ neuropeptide cross-interactions^{10,12–14,17,18,26,27,32,41,42} and show that the premise of the least studied NKA- $\text{A}\beta$ cross-interaction is not unlikely, and that it should be further considered to understand the pathophysiological implications in AD and neurodegenerative disorders.

Here, we show the molecular mechanisms of the NKA- $\text{A}\beta_{1-42}$ cross-interaction. Our study on NKA leads to the following conclusions: (1) NKA influences the formation of the cross- β structure by shielding aromatic and hydrophobic interactions between $\text{A}\beta$ monomers in a concentration-dependent manner. (2) NKA efficiently affects the initial seeding of the formation of early-stage nonfibrillar $\text{A}\beta$ dimers at both $\text{A}\beta$:NKA ratios of 1:1 and 2:1, and the role of the single Phe in NKA is predominant. NKA establishes stable aromatic, hydrophobic, and electrostatic interactions with an $\text{A}\beta$ monomer, and the Trp substitution is not as efficient. (3) The computational observations agree with *in vitro* ThT aggregation kinetics and cellular viability experiments. As a global conclusion, strategic integration of experimental and computational methodologies is required to overcome existing challenges associated with amyloid polymorphism and the relatively brief lifetimes of specific amyloid structures.

Limitations of the study

The results presented here point to NKA as a relevant player in the development of AD, and given the amyloid-TKs relationship, further molecular and mechanistic studies on NKA-amyloid signaling pathways at the brain-gut axis level are required. Altogether, these findings could set the basis for the design of future inhibitory peptides as therapeutic tools in AD.

RESOURCE AVAILABILITY

Lead contact

Further information and requests for resources and reagents should be directed to and will be fulfilled by the lead contact, Alex Perálvarez-Marín, Ph.D. (alex.peralvarez@uab.cat).

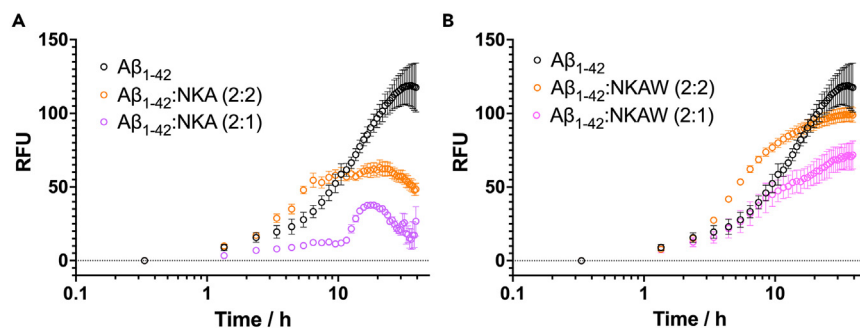


Figure 6. $\text{A}\beta_{1-42}$ ThT aggregation kinetics

$\text{A}\beta_{1-42}$ peptide fibrillation kinetics in the presence of NKA (A) and NKAW (B) peptides at different peptide ratios. 12 μM monomeric $\text{A}\beta_{1-42}$ peptides were incubated in 10 mM sodium phosphate buffer pH 7.4 and 40 μM ThT at +37°C under quiescent conditions in the absence and presence of 6 (2:1) or 12 μM (2:2) NKA or NKAW. The average \pm SEM for each condition calculated from three replicates is shown.

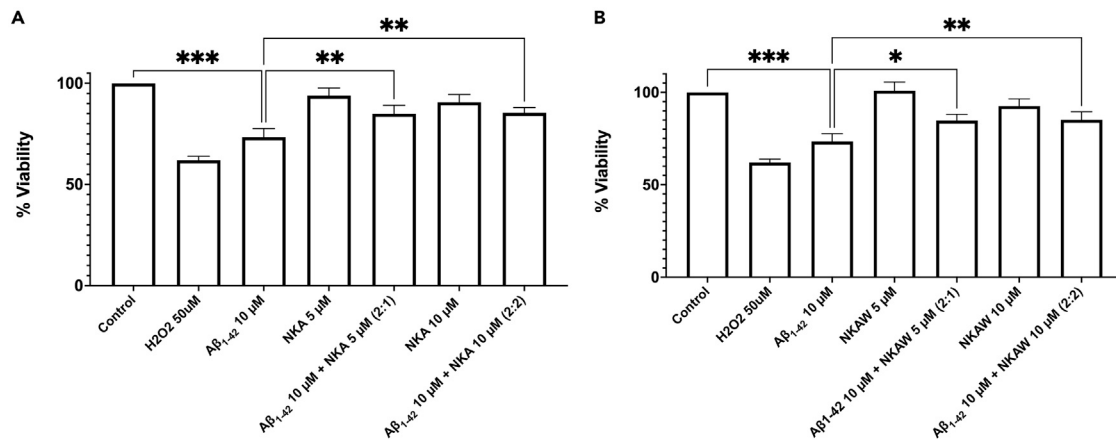


Figure 7. Amyloid-induced cell toxicity in SH-SY5Y cells

The effect on cell viability of Ab₁₋₄₂ and NKA (A) and NKAW (B) was compared to untreated cells and is represented as the average of at least three independent experiments \pm SEM. The effect on cell viability of samples from Ab₁₋₄₂ incubated with NKA and NKAW at two distinct concentrations (Ab₄₀:NKA/NKAW 10 μM:5 μM and 10 μM:10 μM) was compared to Ab₁₋₄₂. Conditions yielding significant differences are indicated (*, $p < 0.01$; **, $p < 0.001$; ***, $p < 0.0001$).

Materials availability

This study did not generate unique reagents.

Data and code availability

- All data reported in this paper will be available from the [lead contact](#) upon request.
- This article does not report original code.
- Any additional information required to reanalyze the data reported in this paper is available from the [lead contact](#) upon request.

ACKNOWLEDGMENTS

Authors acknowledge financial support by the Spanish Government Grant PID2020-120222GB-I00 (to A.P.-M.) funded by MCIN/AEI/10.13039/501100011033, Ministerio de Universidades Margarita Salas Award (MGSD2021-10 to M.L.-M.), and Universitat Autònoma de Barcelona predoctoral fellowship (B21P0033 to E.C.-H.).

AUTHOR CONTRIBUTIONS

Conceptualization, M.L.-M. and A.P.-M.; methodology, A.P.-M. and M.L.-M.; investigation, M.H., E.C.-H., M.L.-M., D.M.-S., and A.P.-M.; writing – original draft, M.H. and A.P.-M.; writing – review and editing, M.H., E.C.-H., M.L.-M., D.M.-S., and A.P.-M.; funding acquisition, A.P.-M.; resources, A.P.-M.; supervision, M.L.-M. and A.P.-M.

DECLARATION OF INTERESTS

The authors declare no competing interests.

STAR METHODS

Detailed methods are provided in the online version of this paper and include the following:

- KEY RESOURCES TABLE
- EXPERIMENTAL MODEL AND STUDY PARTICIPANT DETAILS
- METHOD DETAILS
 - Peptide-peptide docking
 - Molecular dynamics simulations and analysis
 - Peptides
 - Sample preparation
 - Circular dichroism measurements
 - Thioflavin T aggregation kinetics
 - Transmission electron microscopy negative staining
 - MTT cell viability assay
- QUANTIFICATION AND STATISTICAL ANALYSIS

SUPPLEMENTAL INFORMATION

Supplemental information can be found online at <https://doi.org/10.1016/j.isci.2024.111187>.

Received: January 31, 2024

Revised: June 26, 2024

Accepted: October 14, 2024

Published: October 16, 2024

REFERENCES

- Burns, A., and Iliffe, S. (2009). Alzheimer's disease. *BMJ* 338, b158.
- Selkoe, D.J., and Hardy, J. (2016). The amyloid hypothesis of Alzheimer's disease at 25 years. *EMBO Mol. Med.* 8, 595–608.
- Aubrey, L.D., Blakeman, B.J.F., Lutter, L., Serpell, C.J., Tuite, M.F., Serpell, L.C., and Xue, W.F. (2020). Quantification of amyloid fibril polymorphism by nano-morphometry reveals the individuality of filament assembly. *Commun. Chem.* 3, 125.
- Hampel, H., Hardy, J., Blennow, K., Chen, C., Perry, G., Kim, S.H., Villemagne, V.L., Aisen, P., Vendruscolo, M., Iwatsubo, T., et al. (2021). The Amyloid- β Pathway in Alzheimer's Disease. *Mol. Psychiatry* 26, 5481–5503.
- Marsh, J., and Alifragis, P. (2018). Synaptic dysfunction in Alzheimer's disease: the effects of amyloid beta on synaptic vesicle dynamics as a novel target for therapeutic intervention. *Neural Regen. Res.* 13, 616–623.
- Sweeney, M.D., Sagare, A.P., and Zlokovic, B.V. (2018). Blood-brain barrier breakdown in Alzheimer disease and other neurodegenerative disorders. *Nat. Rev. Neurol.* 14, 133–150.
- Bai, R., Guo, J., Ye, X.-Y., Xie, Y., and Xie, T. (2022). Oxidative stress: The core pathogenesis and mechanism of Alzheimer's disease. *Ageing Res. Rev.* 77, 101619.
- Maynard, C.J., Bush, A.I., Masters, C.L., Cappai, R., and Li, Q.-X. (2005). Metals and amyloid- β in Alzheimer's disease. *Int. J. Exp. Pathol.* 86, 147–159.
- Zimbone, S., Giuffrida, M.L., Sabatino, G., Di Natale, G., Tosto, R., Consoli, G.M.L., Milardi, D., Pappalardo, G., and Sciacca, M.F.M. (2023). A β 8-20 Fragment as an Anti-Fibrillrogenic and Neuroprotective Agent: Advancing toward Efficient Alzheimer's Disease Treatment. *ACS Chem. Neurosci.* 14, 1126–1136.
- Loch, R.A., Wang, H., Perálvarez-Marín, A., Berger, P., Nielsen, H., Chroni, A., and Luo, J. (2023). Cross interactions between Apolipoprotein E and amyloid proteins in neurodegenerative diseases. *Comput. Struct. Biotechnol. J.* 21, 1189–1204.
- Petrella, C., Di Certo, M.G., Barbato, C., Gabanella, F., Ralli, M., Greco, A., Possenti, R., and Severini, C. (2019). Neuropeptides in Alzheimer's Disease: An Update. *Curr. Alzheimer Res.* 16, 544–558.
- Luo, J., Wärmländer, S.K., Gräslund, A., and Abrahams, J.P. (2016). Cross-interactions between the Alzheimer Disease Amyloid- β Peptide and Other Amyloid Proteins: A Further Aspect of the Amyloid Cascade Hypothesis. *J. Biol. Chem.* 291, 16485–16493.
- Gallego-Villarejo, L., Wallin, C., Król, S., Enrich-Bengoa, J., Suades, A., Aguilera-Arzo, M., Gomara, M.J., Haro, I., Wärmländer, S., Muñoz, F.J., et al. (2022). Big dynorphin is a neuroprotector scaffold against amyloid β -peptide aggregation and cell toxicity. *Comput. Struct. Biotechnol. J.* 20, 5672–5679.
- Press-Sandler, O., and Miller, Y. (2020). Assessments of the Effect of Neurokinin B on Toxic A β Aggregates in Alzheimer's Disease with the Molecular Mechanisms' Action. *ACS Chem. Neurosci.* 11, 3418–3429.
- Qiu, P., Li, D., Xiao, C., Xu, F., Chen, X., Chang, Y., Liu, L., Zhang, L., Zhao, Q., and Chen, Y. (2023). The Eph/ephrin system symphony of gut inflammation. *Pharmacol. Res.* 197, 106976.
- Martin, C.R., Osadchy, V., Kalani, A., and Mayer, E.A. (2018). The Brain-Gut-Microbiome Axis. *Cell. Mol. Gastroenterol. Hepatol.* 6, 133–148.
- Liu, X., Ganguly, P., Jin, Y., Jhatro, M.J., Shea, J.E., Buratto, S.K., and Bowers, M.T. (2022). Tachykinin Neuropeptides and Amyloid β (25–35) Assembly: Friend or Foe? *J. Am. Chem. Soc.* 144, 14614–14626.
- Chen, X.-Y., Du, Y.-F., and Chen, L. (2018). Neuropeptides Exert Neuroprotective Effects in Alzheimer's Disease. *Front. Mol. Neurosci.* 11, 493.
- Severini, C., Improta, G., Falconieri-Erspamer, G., Salvadori, S., and Erspamer, V. (2002). The Tachykinin Peptide Family. *Pharmacol. Rev.* 54, 285–322.
- Otsuka, M., and Yoshioka, K. (1993). Neurotransmitter functions of mammalian tachykinins. *Physiol. Rev.* 73, 229–308.
- Steinhoff, M.S., von Mentzer, B., Geppetti, P., Pothoulakis, C., and Bunnett, N.W. (2014). Tachykinins and Their Receptors: Contributions to Physiological Control and the Mechanisms of Disease. *Physiol. Rev.* 94, 265–301.
- Holzer, P., and Farzi, A. (2014). Neuropeptides and the Microbiota-Gut-Brain Axis. *Adv. Exp. Med. Biol.* 817, 195–219. https://doi.org/10.1007/978-1-4939-0897-4_9.
- Munekata, E., Kubo, K., Tanaka, H., and Osaka, F. (1987). Structure-activity studies of heptapeptide derivatives related to substance P, neurokinin A, B and other tachykinins on smooth muscles. *Peptides (N.Y.)* 8, 169–173.
- Martinez, M., Frank, A., and Hernanz, A. (1993). Relationship of interleukin-1 β and β 2-microglobulin with neuropeptides in cerebrospinal fluid of patients with dementia of the Alzheimer type. *J. Neuroimmunol.* 48, 235–240.
- Perry, E.K., Blessed, G., Tomlinson, B.E., Perry, R.H., Crow, T.J., Cross, A.J., Dockray, G.J., Dimaline, R., and Arregui, A. (1981). Neurochemical activities in human temporal lobe related to aging and Alzheimer-type changes. *Neurobiol. Aging* 2, 251–256.
- Mantha, A.K., Moorthy, K., Cowski, S.M., and Baquer, N.Z. (2006). Neuroprotective Role of Neurokinin B (NKB) on β -amyloid (25–35) Induced Toxicity in Aging Rat Brain Synaptosomes: Involvement in Oxidative Stress and Excitotoxicity. *Biogerontology* 7, 1–17.
- Flashner, E., Raviv, U., and Friedler, A. (2011). The effect of tachykinin neuropeptides on amyloid β aggregation. *Biochem. Biophys. Res. Commun.* 407, 13–17.
- Calvo, N., Reiriz, J., Pérez-Navarro, E., and Alberch, J. (1996). Tachykinins protect cholinergic neurons from quinolinic acid excitotoxicity in striatal cultures. *Brain Res.* 740, 323–328.
- Teuchner, B., Dimmer, A., Troger, J., Fischer-Colbrie, R., Schmid, E., Kieselbach, G., Dietrich, H., and Bechrakis, N. (2010). Secretoneurin and the tachykinins substance P and neurokinin-A/B in NMDA-induced excitotoxicity in the rat retina. *Regul. Pept.* 165, 123–127.
- Salthun-Lassalle, B., Traver, S., Hirsch, E.C., Michel, P.P., Substance, P., and Neurokinins, A. and B. (2005). Synthetic Tachykinin Peptides Protect Mesencephalic Dopaminergic Neurons in Culture via an Activity-Dependent Mechanism. *Mol. Pharmacol.* 68, 1214–1224.
- Chen, L.W., Yung, K.K.L., and Chan, Y.S. (2004). Neurokinin Peptides and Neurokinin Receptors as Potential Therapeutic Intervention Targets of Basal Ganglia in the Prevention and Treatment of Parkinsons Disease. *Curr. Drug Targets* 5, 197–206.
- Severini, C., Petrella, C., and Calissano, P. (2016). Substance P and Alzheimer's Disease: Emerging Novel Roles. *Curr. Alzheimer Res.* 13, 964–972.
- Nässel, D.R., Zandawala, M., Kawada, T., and Satake, H. (2019). Tachykinins: Neuropeptides That Are Ancient, Diverse, Widespread and Functionally Pleiotropic. *Front. Neurosci.* 13, 1262.
- Sun, W., Yuan, Q., Zhang, H., Yang, F., Ling, S., Luo, Y., Lv, P., Eric Xu, H., Tian, C., Yin, W., and Shi, P. (2022). Structural insights into the activation of neurokinin 2 receptor by neurokinin A. *Cell Discov.* 8, 72.
- Claudio dos Santos, J.C., Lima, M.P.P., Brito, G.A.d.C., and Viana, G.S.d.B. (2023). Role of enteric glia and microbiota-gut-brain axis in parkinson disease pathogenesis. *Ageing Res. Rev.* 84, 101812.
- Thomasi, B., Valdetaro, L., Ricciardi, M.C., Gonçalves de Carvalho, M., Fialho Tavares, I., and Tavares-Gomes, A.L. (2023). Enteric glia as a player of gut-brain interactions during Parkinson's disease. *Front. Neurosci.* 17, 1281710.
- Gasteiger, E., Hoogland, C., Gattiker, A., Duvaud, S.E., Wilkins, M.R., Appel, R.D., and Bairoch, A. (2005). Protein Identification and Analysis Tools on the ExPASy Server. In *The Proteomics Protocols Handbook*, J.M. Walker, ed. (Humana Press), pp. 571–607. <https://doi.org/10.1385/1-59259-890-0:571>.
- Côté, S., Laghaei, R., Derreumaux, P., and Mousseau, N. (2012). Distinct Dimerization for Various Alloforms of the Amyloid-Beta Protein: A β 1-40, A β 1-42, and A β 1-40 (D23N). *J. Phys. Chem. B* 116, 4043–4055.
- Ma, B., and Nussinov, R. (2007). Trp/Met/Phe Hot Spots in Protein-Protein Interactions: Potential Targets in Drug Design. *Curr. Top. Med. Chem.* 7, 999–1005.
- Gazit, E. (2002). A possible role for π -stacking in the self-assembly of amyloid fibrils. *Faseb J.* 16, 77–83.
- Singh, P.K., and Maji, S.K. (2012). Amyloid-Like Fibril Formation by Tachykinin

- Neuropeptides and Its Relevance to Amyloid β -Protein Aggregation and Toxicity. *Cell Biochem. Biophys.* 64, 29–44.
42. Yankner, B.A., Duffy, L.K., and Kirschner, D.A. (1990). Neurotrophic and Neurotoxic Effects of Amyloid β Protein: Reversal by Tachykinin Neuropeptides. *Science* 250, 279–282.
43. Luo, J., and Abrahams, J.P. (2014). Cyclic Peptides as Inhibitors of Amyloid Fibrillation. *Chem. Eur. J.* 20, 2410–2419.
44. Valls-Comamala, V., Guivernau, B., Bonet, J., Puig, M., Peralvarez-Marín, A., Palmer, E., Fernández-Busquets, X., Altafaj, X., Tajes, M., Puig-Pijoan, A., et al. (2017). The antigen-binding fragment of human gamma immunoglobulin prevents amyloid β -peptide folding into β -sheet to form oligomers. *Oncotarget* 8, 41154–41165.
45. Heinig, M., and Frishman, D. (2004). STRIDE: a web server for secondary structure assignment from known atomic coordinates of proteins. *Nucleic Acids Res.* 32, W500–W502.
46. Chaudhury, S., Berrodo, M., Weitzner, B.D., Muthu, P., Bergman, H., and Gray, J.J. (2011). Benchmarking and Analysis of Protein Docking Performance in Rosetta v3.2. *PLoS One* 6, e22477.
47. Pettersen, E.F., Goddard, T.D., Huang, C.C., Couch, G.S., Greenblatt, D.M., Meng, E.C., and Ferrin, T.E. (2004). UCSF Chimera—A visualization system for exploratory research and analysis. *J. Comput. Chem.* 25, 1605–1612.
48. Hosseini-zadeh, P., Bhardwaj, G., Mulligan, V.K., Shortridge, M.D., Craven, T.W., Pardo-Avila, F., Rettie, S.A., Kim, D.E., Silva, D.A., Ibrahim, Y.M., et al. (2017). Comprehensive computational design of ordered peptide macrocycles. *Science* 358, 1461–1466.
49. Huang, J., Rauscher, S., Nawrocki, G., Ran, T., Feig, M., de Groot, B.L., Grubmüller, H., and MacKerell, A.D., Jr. (2017). CHARMM36m: an improved force field for folded and intrinsically disordered proteins. *Nat. Methods* 14, 71–73.
50. McGibbon, R.T., Beauchamp, K.A., Harrigan, M.P., Klein, C., Swails, J.M., Hernández, C.X., Schwantes, C.R., Wang, L.P., Lane, T.J., and Pande, V.S. (2015). MDTraj: A Modern Open Library for the Analysis of Molecular Dynamics Trajectories. *Biophys. J.* 109, 1528–1532.
51. Phillips, J.C., Braun, R., Wang, W., Gumbart, J., Tajkhorshid, E., Villa, E., Chipot, C., Skeel, R.D., Kalé, L., and Schulten, K. (2005). Scalable molecular dynamics with NAMD. *J. Comput. Chem.* 26, 1781–1802.
52. Wahlström, A., Hugonin, L., Perálvarez-Marín, A., Jarvet, J., and Gräslund, A. (2008). Secondary structure conversions of Alzheimer's $\text{A}\beta(1-40)$ peptide induced by membrane-mimicking detergents. *FEBS J.* 275, 5117–5128.
53. Perálvarez-Marín, A., Mateos, L., Zhang, C., Singh, S., Cedazo-Minguez, A., Visa, N., Morozova-Roche, L., Gräslund, A., and Barth, A. (2009). Influence of Residue 22 on the Folding, Aggregation Profile, and Toxicity of the Alzheimer's Amyloid β Peptide. *Biophys. J.* 97, 277–285.

STAR★METHODS

KEY RESOURCES TABLE

REAGENT or RESOURCE	SOURCE	IDENTIFIER
Chemicals, peptides, and recombinant proteins		
A β ₁₋₄₂ peptide	AlexoTech (Umeå, Sweden)	AB-251
Critical commercial assays		
Thioflavin T	Sigma-Aldrich	T3516
3-(4,5-dimethylthiazol-2-yl)-2,5-diphenyltetrazolium bromide (MTT)	Thermo Fisher Scientific	M6494
Deposited data		
A β ₁₋₄₂ helical structure	Protein DataBank	1IYT
A β ₁₋₄₂ solution structure	Protein DataBank	6SZF
NKA structure	Protein DataBank	1N6T
Experimental models: cell lines		
SH-SY5Y Human neuroblastoma cell line	ATCC	CRL-2266
Software and algorithms		
Digital Micrograph software package	(Gatan, Pleasanton, CA)	https://www.gatan.com/
R software	https://cran.r-project.org/	R 4.4.1
UCSF Chimera	https://www.cgl.ucsf.edu/chimera/	Chimera 1.15
STRIDE	Heinig and Frishman ⁴⁵	
Molecular Dynamics trajectory analysis code	This paper	https://github.com/APMlab-memb/2024_NKA_aBeta42.git

EXPERIMENTAL MODEL AND STUDY PARTICIPANT DETAILS

Commercial SH-SY5Y cell line (ATCC CRL-2266) has been used in this study and tested negative for *Mycoplasma*. For all related experiments SH-SY5Y cells (from liquid N₂ storage) were used as the starting material. The experiments to assess cell viability were performed in triplicates for each experimental condition described in three (N = 3) independent experiments.

METHOD DETAILS

Peptide-peptide docking

Global docking was performed using the Rosetta docking protocol.⁴⁶ Input structures for A β ₁₋₄₂ – Protein DataBank (PDB) codes for random coil (PDB: 6SZF, peptide in solution) and helical (PDB: 1IYT, peptide in bicelles) structures, and NKA (PDB: 1N6T) - were retrieved from the Protein DataBank, whereas NKAW structure was obtained by computationally replacing F6 with W6 with UCSF Chimera swapaa command⁴⁷ using Dunbrack's rotamer library. Both NKA and NKAW peptides were acetylated at the C-terminus. Rosetta's local refinement was used after completion of global docking to correct possible clashes present at the interaction interface. Finally, Rosetta's energy-based clustering algorithm⁴⁸ was used, taking the centroid of the most energetically favorable clusters as input structures for molecular dynamics simulations (MDs).

Molecular dynamics simulations and analysis

NKA/NKAW: A β ₁₋₄₂ systems and A β ₁₋₄₂ only systems were prepared for MD simulations using the CHARMM36m force field⁴⁹ and TIP3P water model. Simulations consisted on 5 000 steepest descent minimization steps, followed by 200 ps of NVT (Number of particles, Volume, and Temperature of the system are kept constant) equilibration, and 1 ns of NPT (Number of particles, Pressure, and Temperature of the system are kept constant) equilibration with positional restraints, after which the imposed restrictions were released to further equilibrate the system in the NPT ensemble for 2 ns. Production runs were performed for 1 μ s, using Berendsen barostat and thermostat for pressure and temperature coupling at 1 bar and 310 K respectively. Particle Mesh Ewald was used for electrostatics. Two different stoichiometries, using helical (1IYT) or random coil (6SZF) as starting A β ₁₋₄₂ structures were simulated for the NKA/NKAW: A β ₁₋₄₂ systems, being 2:2 (2 A β ₁₋₄₂ molecules: 2 NKA/NKAW molecules), and 2:1 (2 A β ₁₋₄₂ molecules, 1 NKA/NKAW molecule), accounting for a total of 12 individual simulations, summing up

to 12 μs of total simulation time. Convergence of the simulations was checked with MDTraj.⁵⁰ Secondary structure conversion analyses during the trajectories were performed using Timeline plugin in VMD,⁵¹ according to the secondary structures defined in STRIDE software.⁴⁵

Peptides

Synthetic human Aβ₁₋₄₂ (DAEFRHDSGYEVHHQKLVFFAEDVGSNKGAIIGLMVGG-VVIA) with a purity of >95% was purchased from AlexoTech (Umeå, Sweden), NKA (HKTDSVGLM-NH₂) and NKAW (HKTDSWVGLM-NH₂) were purchased from pepMic Co., Ltd (Jiangsu, China).

Sample preparation

Aβ₁₋₄₂ samples with high-monomer content were prepared by dissolving Aβ₁₋₄₂ in 20 mM NaOH, at a concentration of 1 mg ml⁻¹ and sonicated at least three times in an ice bath.⁵² Peptide samples were snap-frozen in liquid nitrogen and kept at -80°C until further use. The Aβ₁₋₄₂ were diluted to the working concentration in 10 mM phosphate buffer at pH 7.2. Incubated samples for CD (Figure S3), were allowed aggregate for 2 h at 37°C. NKA and NKAW peptides were dissolved directly in 10 mM sodium phosphate buffer pH 7.2. The peptide concentration was determined by weight or spectrophotometrically by absorbance at 280 nm.

Circular dichroism measurements

The far-UV CD spectra (190–250 nm) of the peptide samples were recorded on a Jasco J-815 CD spectrometer (Halifax, Canada) spectropolarimeter. The calibration of the instrument was done prior to each measurement. All measurements were performed at 25°C through a 1 mm path length quartz cuvette. Five scans were recorded and averaged for each spectrum. Peptide concentration used in all experiments was 100 μM in sodium phosphate buffer (10 mM, pH 7.2). For incubated samples containing Aβ₁₋₄₂ peptide, concentrations were reduced to match the concentrations used in ThT experiments, and for that 10 scans were recorded and averaged for each sample.

Thioflavin T aggregation kinetics

Aβ₁₋₄₂ samples were prepared in ice at final concentration of 12 μM in 10 mM sodium phosphate buffer, pH 7.4., 10 mM sodium phosphate buffer pH 7.4, and 40 μM Thioflavin T (ThT, Sigma Aldrich, Cat. N. T3516). The aggregation kinetics were monitored in a 96-well microplate (non-treated) where each well was loaded with 100 μL solutions of mastermix, 12 μM Aβ₁₋₄₂ and 6 μM NKA or NKAW, (2:1, Aβ₁₋₄₂:NKA/NKAW), and 12 μM Aβ₁₋₄₂ and 12 μM NKA or NKAW (2:2, Aβ₁₋₄₂:NKA/NKAW). Peptide samples were loaded to the microplate from lower to higher concentrations. The microplate was covered with a plastic film before being inserted into the microplate reader. The fluorescence intensity was measured in triplicates using a 440 nm excitation filter and a 480 nm emission filter at 37°C with 86 rpm double orbital shake (before each cycle) in a FLUOstar Optima microplate reader (BMG LABTECH, Germany). The plots correspond to three independent experiments.

For the ThT fluorescence kinetic traces analysis, sigmoidal curve fitting based on Equation 1 determining the parameters aggregation half-time, $\tau_{1/2}$ and the maximum growth rate (r_{max}) were performed.

$$F(t) = F_0 + \frac{A}{1+\exp[r_{max}(\tau_1) - t]} \quad (\text{Equation 1})$$

Where F_0 is the fluorescence signal intensity baseline, A is the fluorescence intensity amplitude, r_{max} is the maximum growth rate and the aggregation half-time ($\tau_{1/2}$) corresponds to when the monomeric Aβ₁₋₄₂ peptide population is half depleted.

Transmission electron microscopy negative staining

For negative staining, the sample was prepared by air-dried method. Briefly, an aliquot of purified VLPs was absorbed by flotation onto freshly glow discharged 400 mesh carbon fil copper grids (22-1MC040-100, Microtano). After standing for 1 min at RT, excess sample was drained carefully off the grid using whatman filter paper n°1. Samples were then stained with 8 μL of uranyl acetate (2%) by incubation for 1 min at room temperature. Excess uranyl acetate was drained off as previously described.⁵³

Grids were observed in a Hitachi TEM operating at an accelerating voltage of 75 kV. Electron micrographs were recorded with a GATAN ES500W CCD using the Digital Micrograph software package (Gatan, Pleasanton, CA).

MTT cell viability assay

Mycoplasma negative Human SH-SY5Y neuroblastoma cells were cultured in DMEM/F12 medium nourished with 1xNEAA and 15% FBS. Cells were grown in a 5% CO₂ humidified atmosphere at 37°C to 80% confluence for a maximum of 20 passages. Differentiated SH-SY5Y cells were exposed to previously prepared mixtures of 10 μM aggregated Aβ₁₋₄₂ with 5 μM and 10 μM NKA and NKAW separately, after 20 h of pre-incubation at 37 °C. Cells were seeded into 96-well plates at a density of 1 · 10⁴ cells/100 μL/well and incubated at 37°C for 24 h. The toxicity rate was evaluated after cells were challenged with the different treatment mixtures after 24 h of incubation. Afterward, 11 μL of 3-(4,5-dimethylthiazol-2-yl)-2,5-diphenyltetrazolium bromide (MTT) solution was added to each well and incubated for

2 h at 37°C. After the reaction stopped, DMSO and absorbance were measured at 570 nm and 655 nm. A 100% viability was considered for control cells.

QUANTIFICATION AND STATISTICAL ANALYSIS

For MTT toxicity comparison one-way analysis of Variance (ANOVA) was performed and corrected by Bonferroni's multiple comparison tests for statistical analysis using R software. Conditions yielding significant differences are indicated (*, $p < 0.01$; **, $p < 0.001$; ***, $p < 0.0001$).